Materials Advances

ROYAL SOCIETY OF CHEMISTRY

PAPER

View Article Online
View Journal | View Issue

Cite this: *Mater. Adv.*, 2024, 5, 6185

Co-delivery of berberine and gold nanoparticles on liposomes for photodynamic therapy against 3D lung cancer cells

Kave Moloudi, Heidi Abrahamse and Blassan P. George *

Lung cancer is the second most common cancer diagnosed and is the leading cause of cancer-related deaths globally. Even though there are established lung cancer treatment options including radiotherapy, chemotherapy, and surgery, it remains a great challenge globally. Hence, it is important to explore new procedures such as photodynamic therapy (PDT) to improve the therapeutic outcomes and/or modify established protocol with conventional approaches. PDT is a non-invasive treatment with considerable outcomes in cancer therapy. During PDT, photosensitizer (PS) agents absorb a certain wavelength of laser light and produce reactive oxygen species (ROS), which kill cancer cells. PS agent is one of the critical elements besides the tissue oxygen level and physical parameters of the laser to acheive high treatment efficiency in PDT. Berberine (BBR) has potential as a PS but its free form has some limitations such as limited tumor targeting, poor water solubility and systemic toxicity. However, the objective of this study is the co-delivery of berberine (BBR) and citrate gold nanoparticles (AuNPs) on liposomes (Lipo@AuNPs@BBR) as a new PS compound for PDT on A549 lung cancer spheroid cells. Our hypothesis was that AuNPs can have a synergistic effect on BBR in the Lipo@AuNPs@BBR complex, resulting in more photodamage in PDT on A549 cells. Moreover, liposmes provide a platform for the co-delivery of BBR and AuNPs to cells. Hence, the Lipo@AuNPs@BBR complex was synthesized *via* the thin-film hydration method, and TEM characterization results showed that the size of the Lipo@AuNPs@BBR complex was 100 nm. Moreover, energy-dispersive X-ray spectroscopy (EDS) confirmed that BBR and AuNPs were co-loaded on liposomes while UV-vis spectroscopy showed that the maximum loading was at concentrations of 14 μM (14%) and 11 μg mL^{-1} (18.33%) for BBR and AuNPs, respectively. Furthermore, the IC_{50} (80 μg mL^{-1}) concentration of the Lipo@AuNPs@BBR complex combined with a 405 nm laser at 15 J cm^{-2} fluency induced cytotoxicity on A549 spheroid cells and resulted in decreasing spheroid cell viability to 34.12%. Finally, the Lipo@AuNPs@BBR complex is not only a potent PS drug in PDT at a safe dose but also considered as a nanotheranositc agent in tumor diagnosis and therapy *in vivo* studies.

Received 18th March 2024,
Accepted 11th June 2024

DOI: 10.1039/d4ma00286e

rsc.li/materials-advances

1. Introduction

Lung cancer is the second most commonly diagnosed cancer and is the leading cause of cancer-related deaths globally.[1] There are two main types of lung cancer: non-small cell lung cancer (NSCLC) and small cell lung cancer (SCLC).[2,3] The risk factors for lung cancer include smoking, exposure to second hand smoke, exposure to radon gas, exposure to asbestos and other carcinogens, and a family history of lung cancer.[4,5] Treatment for lung cancer depends on the type and stage of the cancer as well as the patient's overall health. Although some treatment options such as surgery, radiation therapy, chemotherapy, targeted therapy, and immunotherapy can be used for lung cancer therapy, the remedy remains a great challenge and the survival rate is low.[6] However, the search for new modalities and strategies continues.

Photodynamic therapy (PDT) is a non-invasive treatment option for lung cancer that uses a photosensitizing agent and a specific wavelength of light to destroy cancer cells.[7,8] In PDT, reactive oxygen species (ROS) play a crucial role in the destruction of cancer cells. When photosensitizer (PS) agents are exposed to specific wavelengths of light, the PS becomes activated and transitions to a higher energy state. Then, the activated PS interacts with molecular oxygen (O_2) present in the surrounding tissue, leading to the formation of singlet oxygen ($^1O_2$). Singlet oxygen is a highly reactive ROS that can cause damage to cellular components. The generated singlet oxygen and other ROS, such as superoxide and hydroxyl radicals, induce oxidative stress within the cancer cells. This oxidative

Laser Research Centre, Faculty of Health Sciences, University of Johannesburg, P.O. Box 17011, Doornfontein 2028, South Africa. E-mail: blassang@uj.ac.za

stress disrupts cellular functions and damages cellular structures, ultimately leading to cell death.[9,10] PDT is typically used for early-stage lung cancer or for palliative care in advanced cases. Additionally, it may be used in combination with other treatments such as surgery, radiation therapy, or chemotherapy.[11,12] However, it may be a good option for patients who cannot undergo surgery or radiation therapy or who want to avoid these more invasive treatments. Even though PDT has been approved by World Health Organization (WHO) for the treatment of some cancers such as head and neck cancer and skin diseases, it has some challenges such as light penetration, hypoxia, the cytotoxicity of PS and lack of efficient uptake photosensitizing agents in cancer cells, inflammation.[13–15] However, researchers have attempted to find new PS drugs with suitable pharmacokinetics properties, stability as well as low toxicity.

Berberine (BBR) is a natural compound found in several plants, such as goldenseal, barberry, and Oregon grape. It has been traditionally used in Chinese medicine to treat various ailments, including bacterial infections, gastrointestinal disorders, and diabetes.[16,17] Recent studies have also shown its potential as an anticancer agent due to its ability to induce apoptosis in cancer cells. Moreover, several studies have shown that BBR has excellent potential in PDT with high absorption light at 344–420 nm wavelength.[18,19] Hence, there are some limitations of using BBR such as low solubility, high toxicity, low bioavailability and low uptake by cancer cells that may limit its use in combination with PDT for cancer treatment.[20,21] Additionally, more research is needed to fully understand the safety and effectiveness of using BBR in cancer PDT. While some studies have shown promising results,[21,22] more clinical trials are needed to determine its efficacy and potential risks. However, the optimal concentration and duration of treatment for BBR in cancer therapy are still being studied. One strategy to compensate the BBR is using other agent in co-delivery. So, some studies have reported that gold nanoparticles (AuNPs) have potential in photo-thermal therapy. AuNPs can absorb light and produce ROS, leading to cancer cell death *via* apoptosis and autophagy pathways.[23,24] To overcome BBR limitations, researchers have developed a nanoformulation of BBR using a combination of polyethylene glycol (PEG) and chitosan.[20,25,26] Polymeric and lipid-based nanoparticles are used for the co-delivery of anticancer co-drugs in delivery and cancer therapy.[27] In order to increase the BBR efficiency and the synergistic effects of citrate AuNPs in PDT, we designed and synthesized a new nanoformulation of BBR and citrate AuNPs (Lipo@AuNPs@BBR) against A549 spheroid cells.

2. Materials and methods

2.1. Materials

BBR chloride (10006427, powder, purity >95%), dimethyl sulfoxide (DMSO), 3-(4,5-dimethylthiazol-2-yl)-2,5-diphenyltetrazolium bromide (MTT) (11465007001), cholesterol (Chol) (C8667), 1,2-distearoyl-*sn*-glycero-3-phosphocholine (DSPC) (P1138-1G), citrate gold nanoparticles (AuNPs) (741957), Gibco Dulbecco's Modified Eagle Medium (DMEM) (D5796), chloroform (C2432), methanol (439193), fetal bovine serum (FBS), phosphate buffered saline (PBS), live-dead cell viability kit (CBA415), 96-well ultra-low attachment plates (174929), and the CellTiter-GloTM 3D luminescence (G968A) Kit were purchased from Sigma (USA) and Thermo Fisher in Johannesburg, South Africa.

2.2. Synthesis of the Lipo@AuNPs@BBR complex

Lipo@AuNPs@BBR were synthesized by the thin-film hydration as well as using the active method.[28,29] Briefly, a mixture of DSPC (80 mg mL^{-1}), Chol (40 mg mL^{-1}) at 2 : 1 ratio, BBR (100 μM or 3.36 mg) were dissolved in organic solvents chloroform and methanol (8 : 2, v/v), then evaporated in a rotary evaporator (60 rpm at temperature 75 °C for 1 h) to form a thin lipid layer; afterward, 1 mL citrate AuNPs (60 μg mL^{-1}) was added for film hydration. Then, the obtained nanoparticles were stored at 8 °C for characterization.

2.3. Characterization of the Lipo@AuNPs@BBR complex

2.3.1. UV-Vis spectrophotometry and determination of the entrapment efficiency (EE) of BBR and AuNPs. To determine the BBR and citrate AuNPs concentration and efficiency entrapped (EE%) in Lipo@AuNPs@BBR complex, UV-Vis spectrophotometry (Jenway, 7315 spectrophotometer) was performed at room temperature. Then, the comparison of the spectra allows a rough estimation of the quantity of absorbed BBR and citrate AuNPs strength of absorption. In short, the spectrum of the prepared solution was measured to obtain the initial concentration of the free form of BBR, citrate AuNPs, in comparison with Lipo@AuNPs@BBR. For this, 5 mg mL^{-1} of Lipo@AuNPs@BBR complex was centrifuged (18 000 rpm for 1 h) and the supernatant was discarded. Then, the UV-vis study was repeated until the sample reported an almost zero absorption on the measured spectrum. For EE, the following formula was used.

$$EE = (\text{the drug loaded in Lip/total drug added to the system}) \times 100\%$$

2.3.2. Size and polydispersity index (PDI). To evaluate the size distribution, surface charge and stability of liposomes, citrate AuNPs, and the Lipo@AuNPs@BBR complex, dynamic light scattering (DLS) was carried out using a Zetasizer Nano-zs (Malvern Instrument, Zetasizer software 7.03, Malvern, UK). Briefly, all samples were diluted with PBS to measure the size and surface charge to obtain the concentrations. Then, the pH values were measured using a SENTRON pH-meter (Titan, Taiwan).

2.3.3. Fourier-transform infrared (FTIR) spectroscopy. The chemical structure of each sample was evaluated with Fourier-transform infrared (FTIR) spectroscopy using a PerkinElmer Spectrum Version 10.03.02. For this purpose, samples including liposome, BBR, citrate AuNPs and Lipo@AuNPs@BBR were dried and freezed in a platinum pan (Olabo, Axiology labs). Then, FTIR measurements were performed for the samples over

the wavenumber range from 4000 to 400 cm after the dispersion of samples in KBr discs.

2.3.4. Microscopy imaging. To evaluate the morphology, size, loading and uniformity of liposome, citrate AuNPs and Lipo@AuNPs@BBR nanostructures, scanning electron microscopy (SEM, VEGA3 TESCAN) and transmission electron microscopy (TEM) were performed. In addition, energy-dispersive X-ray spectroscopy (EDS) was used for confirming the drug loading on the liposome.

2.3.5. *In vitro* dual-drug release (BBR and AuNPs) from the Lipo@AuNPs@BBR complex. The dialysis technique was carried out to study the *in vitro* release of BBR and AuNPs from the Lipo@AuNPs@BBR complex in phosphate buffered saline (PBS) (pH 7.4) at 37 °C. About 80 μg mL^{-1} of the Lipo@AuNPs@BBR complex was added into the dialysis tube in a thermo-controlled shaker with a stirring speed of 200 rpm at 37 °C for 24 h. Then, the samples were centrifuged at 18 000 rpm for 10 min. The supernatants were collected and BBR and AuNPs concentrations were determined by UV-Vis spectrophotometry at various time intervals (0, 4, 8, 12, 16, 20 and 24 h).

2.3.6. Spheroids uptake and penetration of the Lipo@AuNPs@BBR complex. To determine the time of uptake and penetration (qualitative penetration) of the NPs in A549 spheroids, we used the technique reported by Durand *et al.* and Tchoryk *et al.*[30,31] Thereafter, an appropriate concentration of Hoechst staining (0.1 μg mL^{-1}) was mixed with 80 μg mL^{-1} of the Lipo@AuNPs@BBR complex for 4 h. Afterward, A549 spheroids were incubated with Hoechst dye and Lipo@AuNPs@BBR for 24 h and then, various images of the spheroids were taken by a fluorescence microscope (Carl Zeiss AXio Z1) fluorescence microscopy (Oberkochen, Germany) at different time intervals (0–24 h).

2.3.7. Cytotoxicity of the free form of BBR, citrate Au NPs and Lipo@AuNPs@BBR complex

2.3.7.1. Cell culture. A549 human lung cancer cells were seeded in 25-flask, including DMEM medium with 10% FBS and 1% penicillin–streptomycin (P4458). After the third passage, the cells were harvested and counted. To best evaluate spheroid formation and growth, the cells were plated at a density of 2×10^3, 4×10^3, 6×10^3 and 1×10^4 cells in 200 μL of growth media per well using 96-well spheroid microplates (Corning Cat. No. 4520). Spheroid cultures were analyzed at 0–10 days using an inverted Olympus microscope (USA).

2.3.7.2. Volume doubling time (VDT) for treatment. About 6×10^3 cells per well were seeded in 96-MW. Every day for 10 days, the diameter of the spheroids was measured and the volume was calculated with the formula: $V = 4/3\pi r^3$, where $\pi = 3.14$ and r is radius. Then, the growth curve was calculated with the formula $V = V_0 \times e^{kt}$, where V is secondary volume, V_0 is primary volume after duration (t), e is Napier's constant (2.71828) and k is gradient of logarithmic phase of curve.

2.3.7.3. Morphology of 2D and spheroid (3D) cells. Post treatment, 2D and 3D cells (spheroids) with free form of BBR (14 μM), citrate AuNPs (11 μg mL^{-1}), Lipo@AuNPs@BBR (80 μg mL^{-1}), and liposome (80 μg mL^{-1}) were subjected to single (dark toxicity) and combination treatment with 405 nm laser at 15 J cm^{-2} (60 mW cm^{-2} for 8 min). Then, the morphology of the monolayer cells (2D) and spheroids (3D) were examined using an inverted light microscope light (Olympus).

2.3.7.4. Cytotoxicity of free form of BBR and citrate AuNPs and co-loaded on liposome in single (dark toxicity) and combination treatment with 405 nm laser irradiation. MTT assay was used to measure the spheroid cells viability treated with the free form of BBR at concentrations of 0–200 μM, citrate AuNPs (0–60 μg mL^{-1}), and Lipo@AuNPs@BBR (0–120 μg mL^{-1}) for one VDT (23.44 ± 1.41 h). In order to prepare single cells, spheroids were disassociated with 300 μL trypsin/EDTA (0.25%) for 5 min, then the medium was discarded, and the cells were washed with PBS and 2×10^4 cells per mL seeded in 96-well polystyrene tissue culture plates. The cells were then placed in a humidified 5% CO_2 incubator at 37 °C for 24 h. After incubation, the medium was removed, and 20 μL aliquots of MTT solution (5 mg mL^{-1} in PBS, Sigma, USA) were added to each well and re-incubated at 37 °C for 4 h. Next, 100 μL of the supernatant culture medium was carefully aspirated, and 100 μL aliquots of DMSO were added to each well to dissolve the formazan crystals, followed by 15 min incubation to dissolve the air bubbles. The culture plate was placed on a microplate reader (PerkinElmer, HH35940080 EN, Madrand, South Africa) and shaken for 15 min, and the absorbance was then measured at 540 nm. Afterward, this process was repeated for the combination treatment of BBR (14 μM), citrate AuNPs (11 μg mL^{-1}), IC_{50} of Lipo@AuNPs@BBR (80 μg mL^{-1}) with 405 nm laser at 15 J cm^{-2} (60 mW cm^{-2} for 8 min). Then, the spheroids were incubated for 24 h and the MTT assay protocol was performed to evaluate the phototoxicity. The amount of color produced is directly proportional to the number of the viable cells. All assays were performed in three replicates for each concentration, and each assay was repeated at least two times. The cell viability rate was calculated as the percentage of MTT absorption as per the equation

$$\%\ \text{survival} = (\text{mean experimental absorbance})/(\text{mean control absorbance}) \times 100.$$

2.3.7.5. Lactate dehydrogenase (LDH) assay. For the LDH assay in A549 spheroid cells by ELISA, after three passages of the culture, 6×10^3 cells per well were seeded in 96-well ultra-low attachment plates (174929). When spheroids reached 300–400 μm diameters, then all groups including the control (cells in dark and cells under laser irradiation), citrate AuNPs (11 μg mL^{-1}), free BBR (14 μM) and 80 μg mL^{-1} (IC_{50}) of Lipo@AuNPs@BBR (contain 11 μg mL^{-1} of citrate AuNPs and 14 μM of BBR) were treated with and without (dark toxicity) laser for VDT. Each treatment was in triplicate and three different experiments were performed. Then, 50 μL of media was transferred to the 96-well plate and 50 μL of lactate

substrate was added and incubated for 30 min in a dark place. Finally, the absorbance measurement was done using a Victor Nivo® multimode plate reader (PerkinElmer, Midrand, South Africa) at 490 nm wavelength.

2.3.7.6. Adenosine triphosphate (ATP) luminescence assay. The CellTiter-GloTM 3D luminescence (Promega, G968A, Madison, WI, USA) Kit was used to determine the intracellular ATP content of the A549 spheroids. Briefly, the spheroids were transferred into microcentrifuge tubes and disintegrated with 300 μL of trypsin/EDTA (0.25%) and pipetted. Thereafter, the cells were centrifuged at 3000 rpm for 5 min and washed with 200 μL of HBSS. Then, the supernatant was discarded and the cells were resuspended in HBSS. In total, 50 μL of the cell suspension for each sample was transferred to an opaque 96-well plate, an equal volume of the ATP substrate was added, and the contents were agitated for 5 min to facilitate reagent penetration, lysis, and ATP recovery. The samples were incubated at 37 °C for half an hour, and the intracellular ATP luminescence was recorded using a Victor Nivo® multimode plate reader (PerkinElmer, Midrand, South Africa).

2.3.7.7. Live/dead assay. A live/dead kit from Sigma (Catalog number: CBA415) was used to visualize the A549 spheroid cells under a fluorescence microscope. According to the kit protocol, the control (cells in dark and cells under laser irradiation only) and treated groups were washed three times with PBS and then stained with 1 μg mL^{-1} of ethidium bromide (EtBr) in conjunction with the same concentration of acridine orange (AO) for 10 min in PBS. Consequently, the spheroid cells were rinsed three times with PBS and the visualized images were taken for various groups using Alexa fluor 488 and EtBr channels under a Carl Zeiss fluorescent microscope using the Zen Pro (3.7) Carl Zeiss software.

2.3.8. Statistical analysis. All the tests were performed three times (n = 3) and the average of the data was taken. Control groups involved in the entire study and all the treated groups were compared to those untreated groups using one-way ANOVA (Tukey test) to determine the statistical significance. Statistical analysis was performed using SPSS (Version 22), and the mean, standard deviation and standard error were ascertained. Statistical significance is defined as a p value less than 0.05 and 0.01 (**$p < 0.01$; *$p < 0.05$). Data are represented as mean ± standard deviation (SD).

3. Results

3.1. Characterization of the Lipo@AuNPs@BBR complex

3.1.1. UV-Vis spectrophotometry. The UV-Vis spectra showed that BBR has three peaks in the range of 250–450 nm, citrate AuNPs presented a peak in 530 nm and liposome has a peak near 210 nm wavelength. Additionally, these peaks have been repeated in the Lipo@AuNPs@BBR complex with low intensity. The maximum concentration co-loading of BBR and citrate AuNPs in the Lipo@AuNPs@BBR complex is 14 μM (14 ± 2%) for BBR and 11 μg mL^{-1} (18.33 ± 3.45%) for citrate AuNPs (Fig. 1).

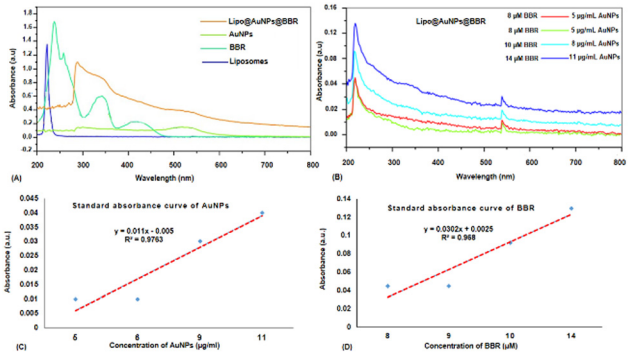

Fig. 1 (A) UV visible spectra for BBR, liposome, citrate AuNPs and Lipo@AuNPs@BBR show their specific peaks. Moreover, (B) the UV-visible spectra illustrates various BBR and citrate AuNPs concentrations loaded on the liposome in the Lipo@AuNPs@BBR complex. (C) and (D) Are the standard absorbance curves of AuNPs and BBR at different concentrations, respectively.

3.1.2. FTIR, DLS and Zetasizer results. FTIR results illustrated that BBR showed four absorbance peaks near 1035, 1105, 1505 and 2850 cm^1. In addition, citrate AuNPs showed four peaks at 1098, 1382, 1638 and 3450 cm^{-1}. Liposome and Lipo@AuNPs@BBR illustrated four same important peaks at 1250, 1459, 1736 and 2907 cm^{-1} (Fig. 2(A)). Dynamic light scattering (DLS) results showed that the surface charge and zeta potential (mV) of liposome, citrate AuNPs and Lipo@AuNPs@BBR was −17.9, −10.7 and −6.54, respectively (Fig. 2(B)–(D)). The results of zeta potential and DLS of size and polydispersity index (PDI), surface charge and stability of the nanoparticle have been summarized in Fig. 3. However, the size of each nanoparticle was measured by a Zetasizer and showed that the size of liposome, AuNPs and Lipo@AuNPs@BBR complex was 320.8 nm, 20.01 nm and 392.1 nm, respectively (Fig. 3(A)–(C)). The zeta potential and Zetasizers are summarized in Fig. 3(D).

3.1.3. Microscopy imaging. The SEM images and energy dispersive spectroscopy (EDS) analysis showed the presence of citrate AuNPs and BBR in the Lipo@AuNPs@BBR complex. In addition, in terms of the morphology, the SEM image showed that the citrate AuNPs are spherical and the BBR drug is in wavy

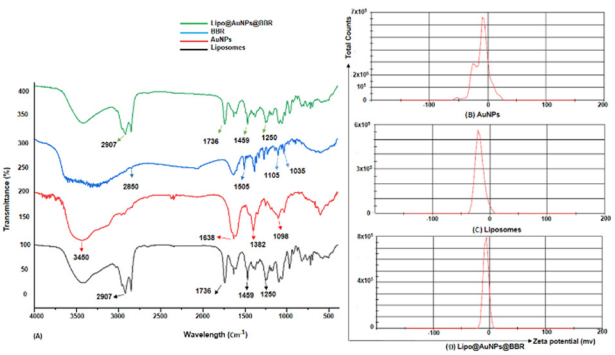

Fig. 2 (A) FTIR spectra of BBR, empty liposomes, citrate AuNPs and Lipo@AuNPs@BBR complex. Zeta potential distribution for citrate AuNPs (B), liposome (C) and Lipo@AuNPs@BBR (D).

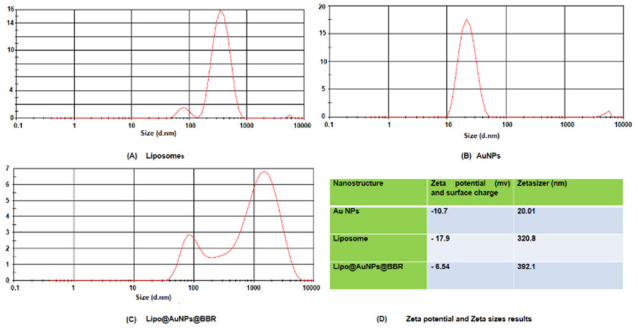

Fig. 3 Zetasizer results of liposome (A), citrate Au NPs (B), and Lipo@AuNPs@BBR (C). Zeta potential and Zetasizers are summarized (D).

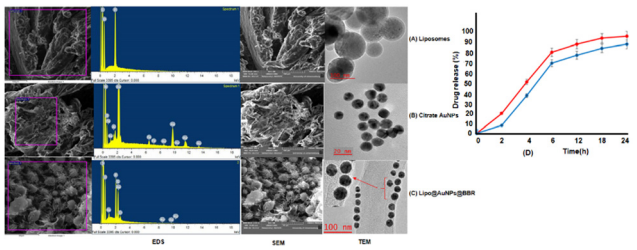

Fig. 4 TEM and SEM images and EDS spectra of liposome (A), citrate AuNPs (B) and Lipo@AuNPs@BBR (C) nanoparticles. (D) The *in vitro* drug release of citrate AuNPs and BBR from the Lipo@AuNPs@BBR complex was measured *via* dialysis in PBS (pH = 7.4) at room temperature for 24 h. As can been seen, citrate AuNPs were released with more speed than BBR from the Lipo@AuNPs@BBR complex.

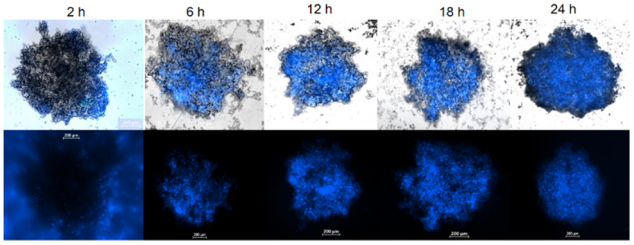

Fig. 5 Time and qualitative penetration of Lipo@AuNPs@BBR mixed with Hoechst dye in the spheroids for 24 h.

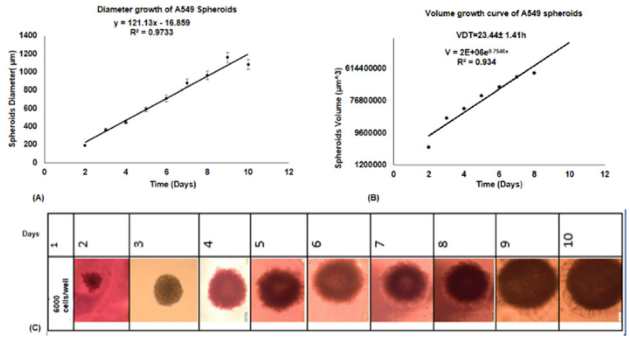

Fig. 6 Diameter (A) and volume growth (B) curve of A549 spheroid cells in 10 days, which shows VDT = 23.44 ± 1.4 h, mean ± SD (n = 3). Also, the shape of the spheroid has been shown in 200 µm resolution (Olympus microscope, USA) (C).

crest shape in the Lipo@AuNPs@BBR complex. The TEM data illustrated that the size of liposome (A), citrate AuNPs (B) and Lipo@AuNPs@BBR complex (C) was 100 nm, 20 nm and 100 nm, respectively (Fig. 4).

3.1.4. *In vitro* dual-drug release (citrate Au NPs and BBR) from the Lipo@AuNPs@BBR complex. The *in vitro* release kinetics of citrate Au NPs and BBR from the Lipo@AuNPs@BBR complex were measured *via* dialysis in PBS (pH = 7.4) at 37 °C for 24 h. It is considerable that the amount of citrate AuNPs and BBR burst release was observed at 2 h, then the release rate also gradually increased. Also, it is clear that the burst release phenomenon for citrate AuNPs is more than BBR. However, as shown in Fig. 4D in the first 4 h, the drug release rate for citrate AuNPs is 52% while this rate for BBR is 38%.

3.1.5. Spheroids uptake and penetration of Lipo@AuNPs@BBR complex. Time and qualitative penetration of Lipo@AuNPs@BBR in spheroids were measured by mixing with 0.1 µg mL^{-1} of Hoechst dye and incubated with spheroids for 24 h. Then, the penetration for dye and Lipo@AuNPs@BBR in the spheroids was followed by a fluorescence microscope. Penetration and whole colored spheroids were visualized after 24 h and are shown in Fig. 5.

3.2. Cellular response

3.2.1. Volume doubling time (VDT) and growth curve. The diameter and volume of A549 spheroid growth curve has been shown in Fig. 6A. The volume doubling time was calculated to be 23.44 ± 1.41 h, which was applied for treatment (Fig. 6B). The maximum diameter of the spheroids reached to near 1200 µm after 10 days.

3.2.2. Morphology of the cells. The morphology of A549 monolayer (2D) cells and spheroids (3D) after the single (dark toxicity) treatment of BBR, citrate Au NP and Lipo@AuNPs@BBR as well as combination treatment with laser visualized and images was captured by an Olympus microscope (USA) in 200 µm resolution (Fig. 7). As can be seen, 2D and 3D images of A549 cells treated by the free form of AuNPs and BBR

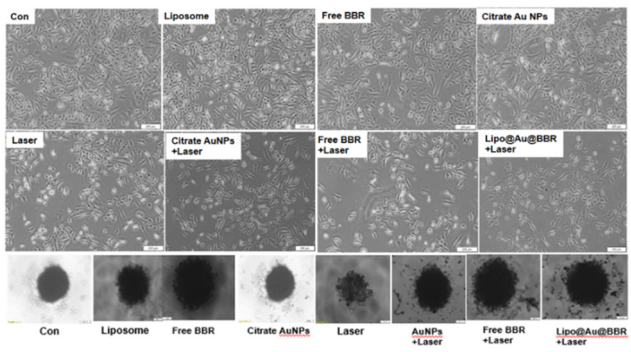

Fig. 7 Morphology of 2D and 3D A549 cells treated with liposome, free BBR (16 µM), citrate AuNPs (11 µg mL^{-1}) and Lipo@AuNPs@BBR (IC_{50} = 80 µg mL^{-1}) alone and in combination treatment with 405 nm laser (15 J cm^{-2}) after VDT (23.44 ± 1.4 h). Treated groups were compared with the control groups visually.

did not show considerable change in the morphology, while in combination with 405 nm laser at 15 J cm^{-2}, it caused dissociation and shrinkages in the cells after VDT treatment. In addition, the IC_{50} concentration of Lipo@AuNPs@BBR in combination treatment with laser caused more photodamages and metastasis in the cells morphology in comparison with the treatment alone.

3.2.3. Cytotoxicity of the free form of AuNPs and BBR and nanoformulation of the Lipo@AuNPs@BBR complex. A549 cells viability and cytotoxicity were investigated by the MTT assay. Fig. 8 shows the viability rate (%) of the treated groups after one VDT. As shown in Fig. 8(A), citrate AuNPs presented the percentage of viability for various groups such as the control, 10, 20, 30, 40, 50 and 60 μg mL^{-1} (100%, 98.6%, 98%, 97.5%, 97.02%, 96.2% and 94.3%, respectively). Furthermore, in Fig. 8(B), a low concentration (<16 μM) of BBR did not show effective toxicity on A549 spheroids, significantly. The viability of different groups including control and the groups treated with 4, 8, 12, 16, 20, 25, 50, 75, 100, 125, 150, 175, 200 μM concentrations of BBR was 100%, 98.5%, 98%, 97.5%, 97.01%, 90.02%, 81.2%, 76.08%, 62.60%, 51.25%, 39.53%, 31.32%, 23.04% and 19.08%, respectively. Afterward, to assess the IC_{50} of Lipo@AuNPs@BBR, A549 spheroid cells were treated with concentrations of 0–120 μg mL^{-1}. The MTT results showed that the IC_{50} of Lipo@AuNPs@BBR was 80 ± 2 μg mL^{-1} in single (dark toxicity) treatment while in combination treatment, it is 60 ± 4 μg mL^{-1} (Fig. 8C).

In addition, Fig. 9 shows the photo-toxicity of the free form of BBR (14 μM), citrate AuNPs (11 μg mL^{-1}) and Lipo@AuNPs@BBR (80 μg mL^{-1}) in single (dark toxicity) and combination treatment with 405 nm laser at an energy of 15 J cm^{-2}. Consequently, the viability of different groups compared with the control was determined. The viability for various groups including the control (cells in dark and cells under laser irradiated only) and single (dark toxicity) treated with BBR (14 μM), single doses of citrate AuNPs (11 μg mL^{-1}) and IC_{50} of Lipo@AuNPs@BBR (80 μg mL^{-1}) contain 14 μM BBR and 11 μg mL^{-1} citrate AuNPs, which was 100%, 98.01%, 97.27% and 52.12%, respectively (Fig. 9A). Moreover, the viability for different groups in combination with the 405 nm laser, including the control, free BBR, citrate Au NPs and Lipo@AuNPs@BBR (80 μg mL^{-1}) was 100%, 90.12%, 77.08%, 84.27% and 34.12%, respectively (Fig. 9B).

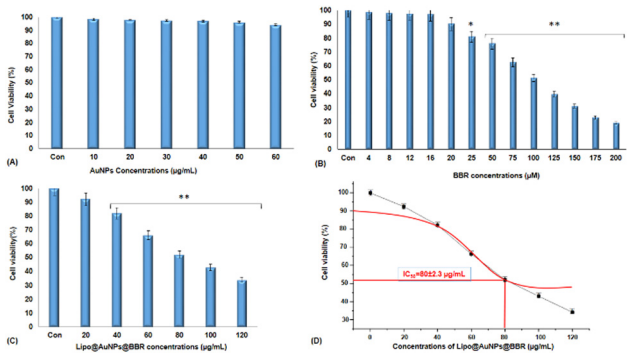

Fig. 8 Cytotoxicity of various concentrations of citrate AuNPs (A), BBR (B) and Lipo@AuNPs@BBR (C) complex on A549 spheroid cells after VDT (23.44 ± 1.4 h) treatment, respectively. (D) IC50 graph of Lipo@AuNPs@BBR. Although the concentration of BBR was low (<16 μM), the cytotoxicity was not significant but the IC_{50} of free BBR and Lipo@AuNPs@BBR was 100 μM and 80 ± 2 μg mL^{-1}, respectively. Data has been reported as mean values ± SD (n = 3) (**p < 0.01; *p < 0.05).

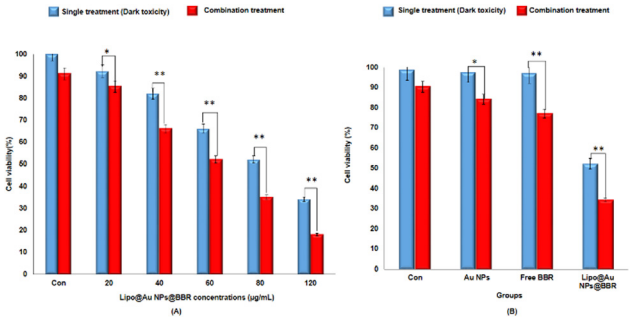

Fig. 9 (A) Cytotoxicity of Lipo@AuNPs@BBR complex with and without ((dark toxicity)) 405 nm laser (15 J cm^{-2}) on A549 spheroid cells after VDT treatment. In the treated groups without (dark toxicity) laser, the IC_{50} of Lipo@AuNPs@BBR was 80 ± 2 μg mL^{-1}, while in combination with laser, it was 60 ± 4 μg mL^{-1}. The IC_{50} of the Lipo@AuNPs@BBR complex at concentrations of 40, 60, 80 and 120 μg mL^{-1} groups was significantly different in comparison to combination with laser but was not significant at low concentration of Lipo@AuNPs@BBR (<20 μg mL^{-1}) with laser treatment. (B) Cytotoxicity of citrate AuNPs (11 μg mL^{-1}), free BBR (14 μM) and Lipo@AuNPs@BBR complex (60 μg mL^{-1} as IC_{50}) alone and in combination with laser is shown in the figure. Data represented as mean values ± SD (n = 3) (**p < 0.01; *p < 0.05).

3.2.4. LDH cytotoxicity. The IC_{50} of Lipo@AuNPs@BBR in single (dark toxicity) and combination treatment with laser caused the release of LDH more than the control (cells in dark and cells under laser irradiated only), BBR and citrate Au NP, significantly. However, the LDH release rate in A549 spheroids treated with 11 μg mL^{-1} of citrate Au NPs, 14 μM of BBR and IC_{50} of Lipo@AuNPs@BBR in comparison with the control (cells only in darkness) was 1.4 (0.56 : 0.4), 1.67 (0.67 : 0.4) and 2.92 times (1.17 : 0.4), respectively. On the other hand, in combination treatment with laser, the LDH rate for various groups including laser alone, citrate Au NPs, BBR and IC_{50} of Lipo@AuNPs@BBR reached 1.67 (0.67 : 0.4), 1.17 (0.66 : 0.56), 1.32 (0.89 : 0.67) and 1.42 (1.67 : 1.17), respectively, in comparison with the single (dark toxicity) treatment, as shown in Fig. 10.

3.2.5. ATP luminescence. The untreated spheroids exhibited a notable amount of luminescence signal, which was positively connected with higher ATP synthesis and eventually, enhanced metabolic activity (Fig. 11(A) and (B)). However, compared to single (dark toxicity) treatment and control groups (cells in dark and cells under laser irradiated only), the spheroids treated with laser irradiation in combination with free BBR, AuNPs, and the IC_{50} of Lipo@AuNPs@BBR displayed appreciable levels of luminescence signal. These findings presented that laser irradiation alone and/or in combination with an IC_{50} of the Lipo@AuNPs@BBR complex exerted inhibitory effects on the spheroids. In other words, the spheroids treated with the photoactivated Lipo@AuNPs@BBR demonstrated a

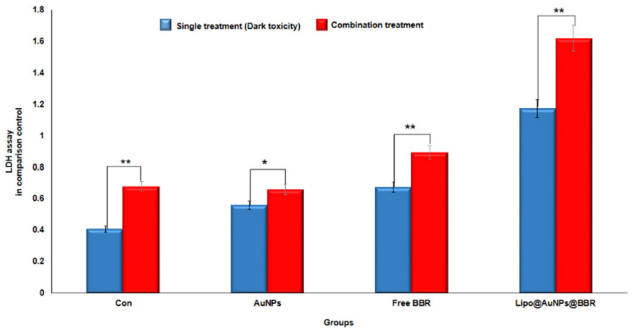

Fig. 10 LDH release level of A549 spheroids in different treated groups in comparison with the control. LDH release in the control group of A549 spheroids has been compared with citrate AuNPs (11 μg mL^{-1}), free BBR (14 μM) and Lipo@AuNPs@BBR complex (IC_{50} = 80 μg mL^{-1}) in single (dark toxicity) and combination with 405 nm laser (15 J cm^{-2}) after VDT.

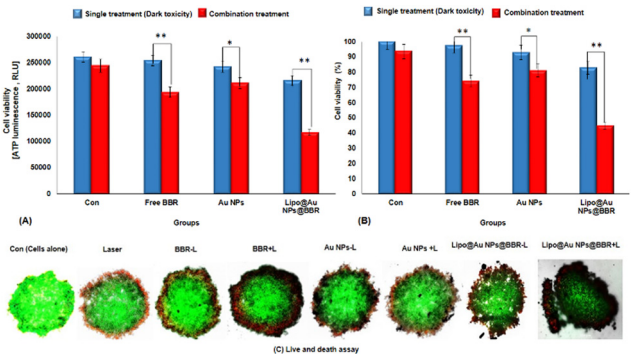

Fig. 11 ATP luminescence assay (A) and cell viability of spheroids after VDT treatment (B), (**$p < 0.01$; *$p < 0.05$). A549 spheroids labelled with AO/EtBr post VDT treatment with (+L) and without laser (−L). Live cells were stained with AO/green while photo-damaged cells were stained with EtBr/red (C).

statistically significant decrease in the ATP production as compared to the untreated control spheroids as well as AuNPs and BBR (**$p < 0.01$; *$p < 0.05$). However, the most potent inhibitory effect was achieved with Lipo@AuNPs@BBR, suggesting that the NPs increased the solubility and cellular uptake of the Lipo@AuNPs@BBR spheroids.

3.2.6. Live and dead assay. The A549 spheroids were stained with 0.1 μg mL^{-1} of AO/EtBr after VDT treatment. Dual staining was visualized under a fluorescence microscope. The AO and EtBr stain can show live and dead cells with green and red color, respectively. Furthermore, the AO stain penetrated in all the spheroid cells and caused the nuclei to emit green fluorescence, while EtBr only permeated the cells with disrupted cytoplasmic membranes and stained the nuclei red.[32] As shown in Fig. 11C, the untreated spheroids (control) did not take up the EtBr staining, resulting in a negative cytotoxicity, while the spheroids treated with (+L) and without (−L) 405 nm laser (15 J cm^{-2}) including laser alone, BBR−L, BBR+L, AuNPs−L, AuNPs+L,Lipo@AuNPs@BBR−L and Lipo@AuNPs@BBR+L, the EtBr stain presented intact cytoplasmic membrane and cell death. However, in the combination group (PDT), spheroids absorbed the EtBr stain more than the control and single treated groups (dark toxicity) due to a compromised cytoplasmic membrane integrity. The IC_{50} of the Lipo@AuNPs@BBR complex with laser caused the most severe photo-damage and dissociation of cells.

4. Discussion

Even though PDT is a non-invasive and highly effective cancer therapy adjuvant to other modalities like chemotherapy, radiation, and target therapy, there are still certain obstacles and limits that need to be overcome, like the PS agent's low solubility, the tumor's hypoxia, and light penetration.[10,33,34] In order to address these problems, a variety of nanoparticles, including AuNPs, have been widely employed in PDT to boost PS delivery in cancer cells, hence encouraging more potent inhibitory effects and better clinical results.[10,35] Furthermore, spheroid cell culture can better predict the *in vivo* responses compared to the monolayer cultures due to the gap-junction of cell–cell interactions and cell–matrix interactions and more physiologically relevant results.[36,37] This study was aimed at investigating the safe co-delivery concentrations of BBR and citrate AuNPs on liposome (Lipo@AuNPs@BBR complex) as the nano-photosensitizer in PDT on A549 spheroid cells. Although BBR has excellent potential as a PS agent in PDT, it has low cancer therapeutic efficiency due to some limitations such as low water solubility and biodegradation.[21,38,39] To overcome these problems, we synthesized the nanoformulation complex from BBR co-loaded with citrate AuNPs on liposome. However, for this purpose, the Lipo@AuNPs@BBR complex was designed and synthesized by the thin-film layer method as well as the active procedure due to the hydrophobic features of the BBR drug.[28,40] UV visible spectroscopy confirmed that liposome presented a peak at 210–220 nm,[41,42] BBR showed three peaks at 250, 350 and 430 nm[43,44] and citrate AuNPs showed a peak at 525–530 nm.[45,46] UV-vis showed that 14 μM (14%) of BBR and 11 μg mL^{-1} (18.33%) of citrate AuNPs had been loaded into the liposome during co-loading, respectively. The free forms of these concentrations of BBR and citrate AuNPs indicated the safe toxicity towards 3D A549 cells. Both BBR and AuNPs had EE% of 14% and 18.33%, respectively, which is lower than those found in the published literature.[47–49] The possible reasons for this could be the poor water solubility and positive charge of cholesterol in liposome, which in turn reduced the amount of BBR that was transmembrane with the same positive charge.[50] FTIR results, on comparing with other studies, showed all specific peaks for free BBR, citrate AuNPs, liposome and Lipo@AuNPs@BBR.[51,52] However, for BBR, the absorption peaks was detected near 1035 (corresponds to C11H, C12H, C13H oop bend), 1105 (corresponds to C–O), 1505 (furyl group) and 2850 cm^{-1} (corresponds to the methoxyl group).[26,51] Also, citrate AuNPs showed four peaks at 1098 (corresponds to C–O stretching), 1382 (corresponds to the symmetric and antisymmetric of COO^{-}), 1638 (C=O stretching) and 3450 cm^{-1} (corresponds to O–H and N–H stretching).[53] Additionally,

liposome and Lipo@AuNPs@BBR illustrated four same peaks at 1250 (C–O of ester groups), 1459 (CH_2 of alkyl groups), 1736 (C═O of ester groups) and 2907 cm^{-1} (symmetric CH_2 stretching of the alkyl groups).[51,52,54,55] Furthermore, DLS data revealed that all samples of nanoparticles have a negative surface charge and were confirmed with other studies.[35,56] PDI and zeta potential (mV) of all the samples are in the acceptable range referencing to other studies.[57] In addition, the EDS analysis of SEM confirmed that BBR and citrate AuNPs were loaded into the liposome and have a wavy crest and spherical shape in the Lipo@AuNPs@BBR complex.[35,58] *In vitro* drug release test from Lipo@AuNPs@BBR was performed with UV-Vis spectroscopy and showed that AuNPs burst release is faster than BBR, which is due to the hydrophilic feature and samples size of AuNPs.[59,60] Finally, the quality penetration of the Lipo@AuNPs@BBR complex in the spheroids was confirmed by Hoechst dye after 24 h, similar to the reports of Durand *et al.* and Tchoryk and co-workers.[30,31] Additionally, the surface charge of nanoparticles is a sign of the stability of the NPs distribution, which reveals the strength of the particles' electrostatic repulsion. This means that because of the strong electric repulsion forces between the molecules, the highly charged particles have a high zeta potential value and are regarded as stable.[61] It's interesting to note that the average hydrodynamic diameter of Lipo@AuNPs@BBR (392.1 ± 0.8 nm, hydrated form) was comparatively larger than their TEM diameter (100 nm, dry form). In contrast to the TEM studies, the Lipo@AuNPs@BBR complex diameter rose when water was present surrounding them during the DLS tests.[62]

The cytotoxicity assay was evaluated by various techniques such as MTT assay, LDH release, ATP assay and live/dead cells following VDT (23.44 ± 1.41 h) for free forms of BBR, citrate AuNPs and Lipo@AuNPs@BBR in single treatment (dark toxicity) and combination with 405 nm laser irradiation. However, first VDT of A549 spheroid cells was calculated from the volume growth curve. VDT helps to present the dynamic behaviors of A549 spheroid cells and allows the spheroid cells to have enough time for the uptake of drugs.[63–65] In agreement, several previous reports, BBR and AuNPs have not shown cytotoxicity in low doses.[48,66] However, according to the MTT results, BBR at a concentration of 0–16 μM and citrate AuNPs at a concentration of 0–60 μg mL^{-1} did not present significant cytotoxicity in comparison with the control group after a VDT. Furthermore, the IC_{50} of Lipo@AuNPs@BBR was about 80 μg mL^{-1} while in combination with the laser, it was 60 μg mL^{-1}. Hence, in comparison with the control groups, free BBR (14 μM) and citrate AuNPs (0–60 μg mL^{-1}) did not present cytotoxicity while the Lipo@AuNPs@BBR group at 80 μg mL^{-1} (IC_{50}) caused cell death, and the cell viability reduced to 52.12%. In addition, the IC_{50} of Lipo@AuNPs@BBR in combination with laser induced a reduction in cell viability to 34.12%. According to the LDH assay results, the IC_{50} of Lipo@AuNPs@BBR in both single (dark toxicity) and combination laser treatment led to a considerable increase in the LDH release compared to the control, BBR, and citrate AuNPs. Also, referring to Fig. 11C, the untreated spheroids exhibited a notable amount of luminous signal, which was positively connected with higher ATP synthesis and metabolic activity.[67] However, the spheroids that were exposed to laser irradiation alone or in combination with free BBR, AuNPs, and the IC_{50} of Lipo@AuNPs@BBR showed less luminescence signal in comparison with the control groups. These findings suggested that laser irradiation alone and or combined with the IC_{50} of the Lipo@AuNPs@BBR complex exerted inhibitory effects on the spheroids. Finally, cell death and photo-damages of the Lipo@AuNPs@BBR complex in PDT was confirmed by live/dead cell assay with a fluorescence microscope. We concluded that the cytotoxicity of Lipo@AuNPs@BBR on A549 spheroid cells in compared to the control, free BBR and citrate AuNPs groups resulted in more uptake and synergistic effects of BBR and Au NPs. All the mentioned experiments above (MTT assay, LDH assay, ATP assay and live/dead assay) confirmed that the Lipo@AuNPs@BBR complex with 405 nm laser (15 J cm^{-2}) induced mitochondrial damage, cells and nucleus membrane damage in A549 cells. Hence, as several articles have reported, the BBR compound has been shown to possess cytotoxic effects when used in PDT. During PTD, BBR is activated by light at a specific wavelength, resulting in ROS generation, which can induce cell death *via* mitochondrial dysfunction, apoptosis and cell cycle arrest.[18,68,69] In contrast, literature reports show that BBR did not show dark toxicity at a low concentration.[68,70]

Compared to free medications, the encapsulation of drugs in liposomes has a number of benefits. Liposomes are easily absorbed by cells because of their colloidal form, which makes them recognizable as foreign particles. Furthermore, liposome physicochemical characteristics, such as membrane charge and particle size, are important factors to target specific tissues and have an impact on the pharmacokinetics and antileishmanial efficacy of medications encapsulated in liposomes.[71,72] In contrast, even though Lipo@AuNPs@BBR demonstrated anti-cancer efficacy and increased the drug concentration in A549 cells when compared to the free drug, it is interesting to mention that the co-loaded drug concentrations on liposomes were significantly lower than the single loading values. In our study, similar to other studies, AuNPs did not show significant cytotoxicity without laser treatment (dark toxicity). In this regard, Keshavarz *et al.* used alginate hydrogel co-loaded with cisplatin and AuNPs (abbreviated as ACA) on the CT 25 cell line, and they reported that the free form of AuNPs does not show significant cytotoxicity in low doses but illustrated significant synergistic effect with cisplatin in cancer therapy.[48] In addition, in a recent study by Vijayakumar, AuNPs were utilized for thermal therapy on MCF-7 cancer cells *in vitro* and *in vivo*. The results showed that AuNPs did not show cytotoxicity at doses less than 20 μg mL^{-1} but in combination with laser, it was effective and induced tumor suppression.[73] Moreover, several studies reported that BBR in single and co-loading with other drugs such as curcumin (Cur) has been used for cancer therapy.[26,74] For instance, Wu. J, *et al.* synthesized the Lipo@Cur@BBR nanocomplex, and their findings showed that EE% was 93.66 ± 3.08 (CUR) and 92.59 ± 5.45 (BBR), while the IC_{50} was 10 μg mL^{-1}.[74] But Sergio *et al.* illustrated that EE% was

17–30% in the single loading of BBR on liposomes (Lipo@BBR) and the IC_{50} was 100 μg mL^{-1}.[26] In the present study, the co-loading of AuNPs and BBR was 18.33% and 14%, respectively. However, IC_{50} was 80 μg mL^{-1}, which is more than that of other studies, and the cytotoxicity of the whole complex depends on the amount of drug loading. Overall, we found that Lipo@AuNPs@BBR complex at 80 μg mL^{-1} concentration could be effective in PDT on A549 lung cancer.

5. Conclusion

The co-loading of BBR and citrate AuNPs on liposome (Lipo@AuNPs@BBR complex) presented low cytotoxicity in single (dark toxicity) treatment on A549 cells, but its synergistic effect in combination PDT is considerable in cancer therapy. Additionally, this single nano-complex (Lipo@AuNPs@BBR complex) well-controlled the optimal dual-drug ratio to dual medications separately, and the single NP showed a greater antitumor activity. Overall, our research solves the challenges associated with designing hydrophobic drug classes, such as berberine, for ratiometric combination therapy. As a result, we have identified this single nanoparticulate delivery platform as an effective and generally safe option for the treatment of human lung cancer. To sum up, this complex due to the exiting AuNPs not only has synergistic effect with BBR in PDT but it can also be employed as a nanotheranostic agent in tumor diagnosis. Finally, it is important to mention that the authors faced a few challenges such the low co-loading of BBR and AuNPs on the liposomes as well as the large size of the nanomaterials in the Zetasizer test in comparison with the TEM results. These limitations should be considered for future *in vivo* studies for more investigations.

Author contributions

K. M. Conceptualization, writing – original draft preparation; B. P. G. and H. A.; writing – review and editing, supervision, funding acquisition. All authors have read and agreed to the published version of the manuscript.

Conflicts of interest

The authors do not have conflicts of interest to disclose.

Acknowledgements

This work is based on the research funded by the South African Research Chairs initiative of the Department of Science and Technology and National Research Foundation (NRF) of South Africa (Grant No. 98337), South African Medical Research Council (Grant No. SAMRC EIP007/2021), as well as grants received from the NRF Research Development Grants for Y-Rated Researchers (Grant No.: 137788), University Research Committee (URC), University of Johannesburg, and the Council for Scientific Industrial Research (CSIR)-National Laser Centre (NLC). The authors sincerely thank the South African Research Chairs initiative of the Department of Science and Technology and the National Research Foundation (NRF) of South Africa, South African Medical Research Council (SAMRC). The research reported in this original article was supported by the South African Medical Research Council (SAMRC) through its Division of Research Capacity Development under the Research Capacity Development Initiative from funding received from the South African National Treasury. The content and findings reported/illustrated are the sole deduction, view, and responsibility of the researchers and do not reflect the official position and sentiments of the SAMRC.

References

1 K. Robien and L. DiPietro, *Chest*, 2024, **165**, 14–15.
2 B. Zhou, R. Zang, M. Zhang, P. Song, L. Liu, F. Bie, Y. Peng, G. Bai and S. Gao, *EBioMedicine*, 2022, **78**, 103951.
3 J. Subramanian, T. Regenbogen, G. Nagaraj, A. Lane, S. Devarakonda, G. Zhou and R. Govindan, *J. Thorac. Oncol.*, 2013, **8**, 860–865.
4 A. M. Saad, M. J. Al-Husseini, H. H. Mohamed, M. A. Alkhayat, M. B. Sonbol and O. Abdel-Rahman, *Porto Biomed. J.*, 2017, **2**, 212.
5 F. Wang, X. Xu, J. Yang, L. Min, S. Liang and Y. Chen, *PLoS One*, 2017, **12**, e0185316.
6 G. S. Jones and D. R. Baldwin, *Clin. Med.*, 2018, **18**, s41.
7 K. Moloudi, H. Abrahamse and B. P. George, *Front. Oncol.*, 2023, **13**, 1225694.
8 K. Moloudi, P. Sarbadhikary, H. Abrahamse and B. P. George, *Antioxidants*, 2023, **12**, 1434.
9 K. Moloudi, H. Abrahamse and B. P. George, *Front. Oncol.*, 2023, **13**, 1225694.
10 K. Moloudi, H. Abrahamse and B. P. George, *Wiley Interdiscip. Rev.: Nanomed. Nanobiotechnol.*, 2024, **16**, e1937.
11 R. Allison, K. Moghissi, G. Downie and K. Dixon, *Photodiagnosis Photodyn. Ther.*, 2011, **8**, 231–239.
12 C. B. Simone II and K. A. Cengel, *Semin. Oncol.*, 2014, **41**, 820–830.
13 M. J. Garland, C. M. Cassidy, D. Woolfson and R. F. Donnelly, *Future Med. Chem.*, 2009, **1**, 667–691.
14 M. M. Kim and A. Darafsheh, *Photochem. Photobiol.*, 2020, **96**, 280–294.
15 D. Van Straten, V. Mashayekhi, H. S. De Bruijn, S. Oliveira and D. J. Robinson, *Cancers*, 2017, **9**, 19.
16 A. Amin, T. Subbaiah and K. Abbasi, *Can. J. Microbiol.*, 1969, **15**, 1067–1076.
17 B. Philogene, J. Arnason, G. Towers, Z. Abramowski, F. Campos, D. Champagne and D. McLachlan, *J. Chem. Ecol.*, 1984, **10**, 115–123.
18 H.-Q. Liu, Y.-W. An, A.-Z. Hu, M.-H. Li and G.-H. Cui, *Open Chem.*, 2019, **17**, 413–421.
19 H. Liu, T. Zheng, Z. Zhou, A. Hu, M. Li, Z. Zhang, G. Yu, H. Feng, Y. An and J. Peng, *RSC Adv.*, 2019, **9**, 10528–10535.

20 Y.-W. An, H.-T. Jin, B. Yuan, J.-C. Wang, C. Wang and H.-Q. Liu, *Oncol. Lett.*, 2021, **21**, 1–10.
21 A. Och, R. Podgórski and R. Nowak, *Toxins*, 2020, **12**, 713.
22 N. L. Andreazza, C. Vevert-Bizet, G. Bourg-Heckly, F. Sureau, M. J. Salvador and S. Bonneau, *Int. J. Pharm.*, 2016, **510**, 240–249.
23 J. Beik, M. Khateri, Z. Khosravi, S. K. Kamrava, S. Kooranifar, H. Ghaznavi and A. Shakeri-Zadeh, *Coord. Chem. Rev.*, 2019, **387**, 299–324.
24 Z. Abed, J. Beik, S. Laurent, N. Eslahi, T. Khani, E. S. Davani, H. Ghaznavi and A. Shakeri-Zadeh, *J. Cancer Res. Clin. Oncol.*, 2019, **145**, 1213–1219.
25 B. F. Floriano, T. Carvalho, T. Z. Lopes, L. A. U. Takahashi, P. Rahal, A. C. Tedesco and M. F. Calmon, *Photodiagnosis Photodyn. Ther.*, 2021, **33**, 102174.
26 S. Comincini, F. Manai, M. Sorrenti, S. Perteghella, C. D'Amato, D. Miele, L. Catenacci and M. C. Bonferoni, *Pharmaceutics*, 2023, **15**, 1078.
27 A. Narmani, R. Jahedi, E. Bakhshian-Dehkordi, S. Ganji, M. Nemati, R. Ghahramani-Asl, K. Moloudi, S. M. Hosseini, H. Bagheri and P. Kesharwani, *Expert Opin. Drug Delivery*, 2023, **20**, 937–954.
28 H. Zhang, *Liposomes: Methods and Protocols*, Springer, 2023, pp. 57–63.
29 H. Zhang, *Liposomes: Methods and protocols*, 2017, 17–22.
30 R. E. Durand, *J. Histochem. Cytochem.*, 1982, **30**, 117–122.
31 A. Tchoryk, V. Taresco, R. H. Argent, M. Ashford, P. R. Gellert, S. Stolnik, A. Grabowska and M. C. Garnett, *Bioconjugate Chem.*, 2019, **30**, 1371–1384.
32 F. Salehi, H. Behboudi, G. Kavoosi and S. K. Ardestani, *Sci. Rep.*, 2017, **7**, 2553.
33 D. Bhattacharya, M. Mukhopadhyay, K. Shivam, S. Tripathy, R. Patra and A. Pramanik, *Biomed. Mater.*, 2023, **8**, 062005.
34 G. Gunaydin, M. E. Gedik and S. Ayan, *Front. Chem.*, 2021, **9**, 691697.
35 K. Moloudi, A. Khani, M. Najafi, R. Azmoonfar, M. Azizi, H. Nekounam, M. Sobhani, S. Laurent and H. Samadian, *Wiley Interdiscip. Rev.: Nanomed. Nanobiotechnol.*, 2023, e1886.
36 K. Moloudi, A. Neshasteriz, A. Hosseini, N. Eyvazzadeh, M. Shomali, S. Eynali, E. Mirzaei and A. Azarnezhad, *Iranian Biomed. J.*, 2017, **21**, 330.
37 M. Ravi, V. Paramesh, S. Kaviya, E. Anuradha and F. P. Solomon, *J. Cell. Physiol.*, 2015, **230**, 16–26.
38 Q. Lu, Y. Fu and H. Li, *Pharmacol. Rep.*, 2022, **74**, 297–309.
39 J. Wang, Q. Qi, Z. Feng, X. Zhang, B. Huang, A. Chen, L. Prestegarden, X. Li and J. Wang, *Oncotarget*, 2016, **7**, 66944.
40 S. K. Sahoo, *Liposomal Encapsulation in Food Science and Technology*, Elsevier, 2023, pp. 39–63.
41 T. A. Nguyen, Q. D. Tang, D. C. T. Doan and M. C. Dang, *Adv. Nat. Sci.: Nanosci. Nanotechnol.*, 2016, **7**, 035003.
42 S. M. El Faramawy and R. A. Rizk, *J. Am. Soc. Sci.*, 2011, **7**, 363–369.
43 Y. Kamal, M. Singh, E. Tamboli, R. Parveen and S. Ahmad, *Acta Chromatogr.*, 2011, **23**, 157–168.
44 L. Yu-Chung, L. Zhe-Rui, T. Lin-Wei, P. Elena, K. Artashes and C. Chia-Liang, *J. Biomed. Photonics Eng.*, 2017, **3**, 10305.
45 S. Makumire, N. Revaprasadu and A. Shonhai, *PLoS One*, 2015, **10**, e0121243.
46 J. C. Mohan, G. Praveen, K. Chennazhi, R. Jayakumar and S. Nair, *J. Exp. Nanosci.*, 2013, **8**, 32–45.
47 X. Ma, X. Sui, C. Liu, H. Li, C. Han, T. Xu, H. Zhang, Y. Zhang, D. Cai and Y. Li, *Colloids Surf., A*, 2023, **673**, 131773.
48 M. Keshavarz, K. Moloudi, R. Paydar, Z. Abed, J. Beik, H. Ghaznavi and A. Shakeri-Zadeh, *J. Biomater. Appl.*, 2018, **33**, 161–169.
49 P. Liu, G. Chen and J. Zhang, *Molecules*, 2022, **27**, 1372.
50 A. Magarkar, V. Dhawan, P. Kallinteri, T. Viitala, M. Elmowafy, T. Róg and A. Bunker, *Sci. Rep.*, 2014, **4**, 5005.
51 F. A. Younis, S. R. Saleh, S. S. A. El-Rahman, A.-S. A. Newairy, M. A. El-Demellawy and D. A. Ghareeb, *Sci. Rep.*, 2022, **12**, 17431.
52 A. Musa, A. H. Elmaidomy, A. M. Sayed, S. I. Alzarea, M. M. Al-Sanea, E. M. Mostafa, O. M. Hendawy, M. A. Abdelgawad, K. A. Youssif and H. Refaat, *Int. J. Nanomed.*, 2021, 3861–3874.
53 P. Wulandari, X. Li, K. Tamada and M. Hara, *J. Nonlinear Opt. Phys. Mater.*, 2008, **17**, 185–192.
54 M. Leona and J. R. Lombardi, *J. Raman Spectrosc.*, 2007, **38**, 853–858.
55 Z. Wang, Y. Tian, H. Zhang, Y. Qin, D. Li, L. Gan and F. Wu, *Int. J. Nanomed.*, 2016, 6485–6497.
56 D. H. Jo, J. H. Kim, T. G. Lee and J. H. Kim, *Nanomedicine*, 2015, **11**, 1603–1611.
57 M. Danaei, M. Dehghankhold, S. Ataei, F. Hasanzadeh Davarani, R. Javanmard, A. Dokhani, S. Khorasani and M. Mozafari, *Pharmaceutics*, 2018, **10**, 57.
58 J. Jia, K. Zhang, X. Zhou, D. Zhou and F. Ge, *Polymers*, 2018, **10**, 1198.
59 L. L. David, A. Daniels, S. Habib and M. Singh, *J. Drug Delivery Sci. Technol.*, 2023, **90**, 105168.
60 A. K. Jain and S. Thareja, *Artif. Cells, Nanomed., Biotechnol.*, 2019, **47**, 524–539.
61 S. S. Imam, S. Alshehri, M. M. Ghoneim, A. Zafar, O. A. Alsaidan, N. K. Alruwaili, S. J. Gilani and M. Rizwanullah, *Polymers*, 2021, **13**, 4036.
62 S.-J. Wu, T.-M. Don, C.-W. Lin and F.-L. Mi, *Mar. Drugs*, 2014, **12**, 5677–5697.
63 H. J. G. Lindström and R. Friedman, *BMC Bioinf.*, 2020, **21**, 1–13.
64 S. Park, S. M. Lee, S. Kim, J.-G. Lee, S. Choi, K.-H. Do and J. B. Seo, *Radiology*, 2020, **295**, 703–712.
65 Y. Wang, M. M. Kheir, Y. Chai, J. Hu, D. Xing, F. Lei and L. Du, *PLoS One*, 2011, **6**, e23495.
66 A. Rauf, T. Abu-Izneid, A. A. Khalil, M. Imran, Z. A. Shah, T. B. Emran, S. Mitra, Z. Khan, F. A. Alhumaydhi and A. S. Aljohani, *Molecules*, 2021, **26**, 7368.
67 N. W. Nkune and H. Abrahamse, *Pharmaceutics*, 2023, **15**, 2264.
68 P. Oliveira, T. Lopes, A. C. Tedesco, P. Rahal and M. Calmon, *Photodiagnosis Photodyn. Ther.*, 2020, **32**, 102045.
69 X. Wang, Q. Gong, C. Song, J. Fang, Y. Yang, X. Liang, X. Huang and J. Liu, *Toxicol. Appl. Pharmacol.*, 2021, **418**, 115484.

70 T. Z. Lopes, F. R. de Moraes, A. C. Tedesco, R. K. Arni, P. Rahal and M. F. Calmon, *Biomed. Pharmacother.*, 2020, **123**, 109794.
71 A. de Souza, D. S. S. Marins, S. L. Mathias, L. M. Monteiro, M. N. Yukuyama, C. B. Scarim, R. Löbenberg and N. A. Bou-Chacra, *Int. J. Pharm.*, 2018, **547**, 421–431.
72 N. Bertrand and J.-C. Leroux, *J. Controlled Release*, 2012, **161**, 152–163.
73 S. Vijayakumar, *Appl. Phys. A*, 2023, **129**, 462.
74 J. Wu, C. Qi, H. Wang, Q. Wang, J. Sun, J. Dong, G. Yu, Z. Gao, B. Zhang and G. Tian, *Front. Pharmacol.*, 2022, **13**, 961788.